Nighttime Image Dehazing Based on Retinex and Dark Channel Prior Using Taylor Series Expansion

Qunfang Tang[1,4], Jie Yang[1], Xiangjian He[2], *Senior Member, IEEE*, Wenjing Jia[2], Qingnian Zhang[3], and Haibo Liu[4]
[1]Hubei Key Laboratory of Broadband Wireless Communication and Sensor Networks, Wuhan University of Technology, Wuhan, China
[2]Global Big Data Technologies Centre (GBDTC), University of Technology Sydney, Ultimo, Australia
[3]School of Transportation, Wuhan University of Technology, Wuhan, China
[4]School of Electrical Information Engineering, Hunan Institute of Technology, Hengyang, China

Haze removal from nighttime images is more difficult compared with daytime image dehazing due to the uneven illumination, low contrast and severe color distortion. In this paper, following the approaches based on Dark channel prior, we propose a simple yet effective approach using Retinex theory and Taylor series expansion for nighttime image dehazing, referred to as 'RDT'. Existing nighttime image dehazing methods do not handle color shift and glow removal very well. In order to address these issues, we first propose to decompose the atmospheric light image from the input image based on the Retinex theory. Taylor series expansion is then introduced for the first time to accurately estimate the pointwise transmission map. Finally, during the following processes of image fusion and color transfer, the atmospheric light image and potential haze-free image are adopted to obtain the final haze-free image. The experimental results on benchmark nighttime haze images demonstrate the superior performance of our proposed RDT dehazing method over the state-of-the-art methods.

***Index Terms*—Nighttime image dehazing, Retinex theory, Taylor series expansion, image fusion, color transfer.**

I. Introduction

IMAGES captured outdoors in fog and haze weather engender the degeneracy phenomenon, such as low contrast or color distortion, which seriously affects the performance of outdoor visual systems. According to Middleton's model [1], a haze image $I(x)$ can be described as a linear combination of a direct attenuation term and a scattering term as:

$$I(x) = J(x)t(x) + A[1 - t(x)] = A\rho(x)t(x) + A[1 - t(x)], \quad (1)$$

where x is a pixel coordinate, $I(x)$ is the observed haze image, $J(x)$ is its haze-free image, A is the global atmospheric light, $\rho(x)$ is a scene albedo, and $t(x) = e^{-\beta d(x)}$ is the transmission map depending on the scattering coefficient β and scene depth $d(x)$. To retrieve the haze-free image $J(x)$, the global atmospheric light A and the transmission map $t(x)$ need to be estimated, which lead to an underdetermined estimation problem.

Based on Middleton's model [1], a number of methods have been proposed to remove haze from single images [2], [3], [4], [5], [6], [7], [8], [9], [10], [11], [12]. The key to their success is based on the above optical model in Eq. 1 and various image priors, *e.g.*, the dark channel prior in [2] and the color attenuation prior in [6]. Although these methods are effective on dehazing daytime images, they are not effective enough when dealing with nighttime haze images. Fig. 1 shows the dehazing results on a nighttime haze image using different methods. The daytime dehazing method [2] has failed to remove haze (see Fig. 1 (b)), and the nighttime dehazing method [13] is erroneous in dealing with glow and produces color distortion(see Fig. 1 (c)). As shown in Fig. 1 (d), our proposed method has obtained good and more natural dehazing effect. The main reason is that the above daytime haze imaging model [1] does not actually suit the nighttime haze scenes [13] and some priors cannot be established either. For instance, the dark channel prior in [2] does not hold for the illuminating conditions of nighttime haze scenes because of multiple artificial light sources (see Fig. 1 (a)).

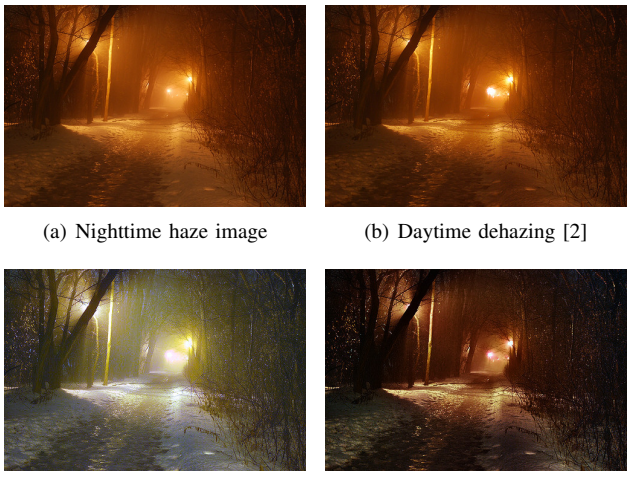

(a) Nighttime haze image (b) Daytime dehazing [2]
(c) Nighttime dehazing [13] (d) Proposed method

Fig. 1: An example of nighttime haze image and the dehazing results obtained with a daytime dehazing method and an existing nighttime dehazing method, and our proposed method.

Recently, some solutions for nighttime haze removal were emerged [13], [14], [15], [16], [17]. In [13], a novel maximum reflectance prior was proposed to process single nighttime haze images. The prior came from a key observation that the local maximum intensities were mainly contributed by the ambient illumination. Using maximum reflectance prior, the ambient illumination and transmission map were estimated to restore a haze-free image. The algorithm may fail to dispose some cases with color distortion such as the regions of grasses or leaves.

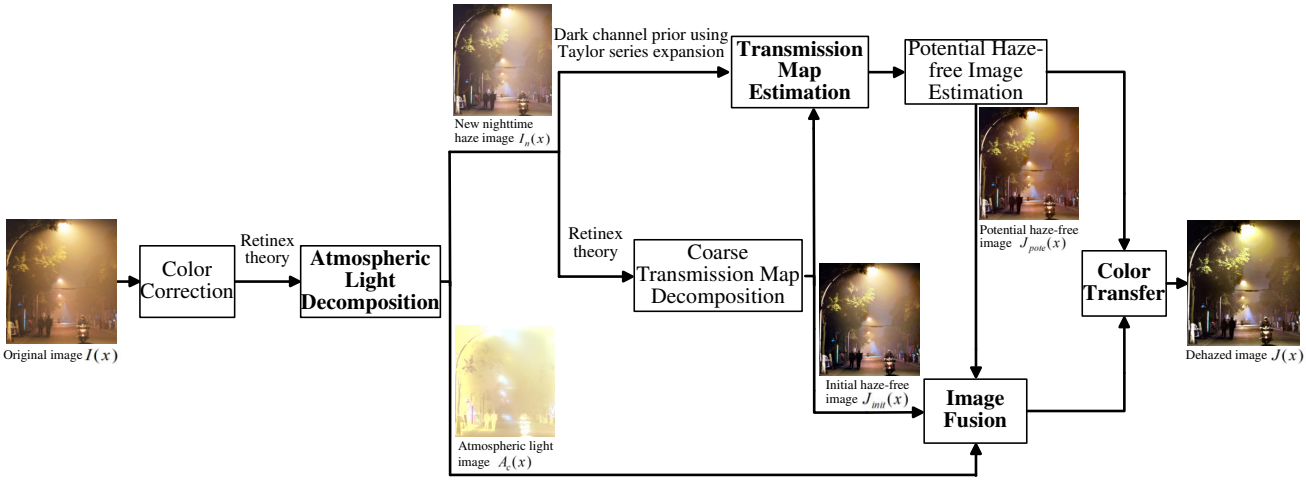

Fig. 2: The flow chart of our proposed method.

Zhang *et al.* [14] proposed a new nighttime dehazing method with illumination estimation. The method, which utilized the Retinex algorithm to estimate and enhance the incident light intensity, adopted the gamma adjustment for color correction, and used the dark channel prior to obtain a haze-free image. Because of the additional post processing, it may result in color distortion. Li *et al.* [15] introduced a new nighttime haze model, which accounted for the varying light sources and their glow. The model regarded the glow as an atmospheric point spread function, and used the layer separation technique in [18] to remove the glow. The method can effectively eliminate the halo artifacts, but the output image appears to be unnatural and is prone to over-enhancing some local areas. Liao *et al.* [16] proposed an end-to-end learning-based solution to remove haze from nighttime images. The solution used a novel model to represent a nighttime haze image, and adopted a Haze Density Prediction Network (HDP-Net) to obtain a haze density map, which was used to generate a haze-free output. However, the dehazing effect of output image is not very obvious and is liable to produce halo effect. Yang *et al.* [17] proposed a novel superpixel-based single image haze removal algorithm for nighttime haze images. Their algorithm utilized the superpixel-based method to compute the value of the atmospheric light and dark channel in the glow-free haze image, which was decomposed from an input nighttime image. Then, the dark channel was used to estimate the transmission map, and an adaptive threshold was added to the transmission map for obtaining a restored image. The algorithm has achieved good results in image haze removal, but it may generate exaggerated intensity of some areas such as artificial light sources and produce color distortion.

In this paper, following the Dark channel prior we propose a simple but effective nighttime haze removal method based on the Retinex theory and Taylor series expansion. For the ease of reference, we refer to this approach as 'RDT' dehazing. As we all know, Retinex [11], [19] is a color vision model mimicking the ability of the Human Visual System to robustly discount varying illuminations when observing a scene under different spectral lighting conditions. In [14], the Retinex algorithm was used to enhance image brightness. Different from the method proposed in [14], our proposed RDT method adopts the Retinex theory to first decompose the atmospheric light from the input image and then uses it to accurately estimate the transmission map so as to dehaze nighttime images. Similar to the methods in [14], [15], our proposed RDT method utilizes the dark channel prior to realize the haze removal process. However, to obtain a more accurate pointwise estimation of the transmission map for nighttime haze images, we for the first time introduce the Taylor series expansion in this process. Finally, to further improve the quality of the restored image both in the aspects of illumination and color, image fusion [20], [21], [22], [23] and color transfer [24] algorithms are adopted in our approach. The quantitative and qualitative comparison with several recent state-of-the-art methods demonstrates that our proposed RDT method is robust and effective.

The remainder of this paper is organized as follows. In Section II, the nighttime haze imaging model is briefly introduced. In Section III, our proposed method is illustrated in details. In Section IV, experiments and results are presented and analyzed. Finally, the conclusion is drawn in Section V.

II. Nighttime Haze Imaging Model

Eq. 1 gives the daytime haze imaging model, but it is inappropriate to describe nighttime haze images due to the presence of artificial light sources. For example, MSCNN-HE [12] was trained on the synthetic dataset which was created based on the daytime haze imaging model. Therefore, it is less effective for the nighttime hazy images or the images with non-uniform atmospheric light and results in some dark region since the inaccuracy of the estimated atmospheric light.

Recently, several nighttime haze imaging models have been proposed [14], [15], [16]. Compared with the daytime haze imaging model in Eq. 1, nighttime dehazing models focus on various artificial light sources and their glow. In our work, we adopt the nighttime haze imaging model in [14], where a haze image is described as:

$$\begin{aligned} I(x) &= J(x)t(x) + A(x)[1 - t(x)] \\ &= A(x)\rho(x)t(x) + A(x)[1 - t(x)], \end{aligned} \tag{2}$$

where $I(x)$, $J(x)$, $\rho(x)$ and $t(x)$ have the same meanings with the ones in Eq. 1.

Compared with the daytime haze imaging model in Eq. 1, the nighttime haze imaging model replaces the global

(a) Bench (b) Building

Fig. 3: Examples of two nighttime haze images. (a) Bench: a color-shift nighttime haze image; (b) Building: a normal nighttime haze image.

atmospheric light A with a pointwise variable $A(x)$, which varies with locations. This is because different artificial light sources in nighttime haze environment generate various colors, which affect the atmospheric light during the scattering process. As we all know, the dark channel prior [2] is a solution to the image dehazing problem as well as Retinex on inverted intensities [11]. For the nighttime hazy image, Retinex is used to estimate the atmospheric light $A(x)$. And Taylor series expansion is introduced to accurately estimate the pointwise transmission map $t(x)$ combined with the dark channel prior [2]. Finally, using $A(x)$ and $t(x)$, we retrieve the haze-free image $J(x)$ from the input nighttime haze image $I(x)$.

III. The Proposed Method

As shown in the flow chart in Fig. 2, our proposed method consists of the following three parts and are detailed in the subsections below. 1) *Atmospheric Light Decomposition*. The shades-of-gray color correction algorithm [25] is first adopted to deal with the nighttime haze image because of the colored artificial light sources, and then Retinex theory is performed on the color-corrected haze image to decompose the atmospheric light image. 2) *Transmission Map Estimation*. A Taylor series expansion is introduced to deduce the transmission map based on the dark channel prior, and the optimized transmission map is used to produce a potential haze-free image. 3) *Image Fusion and Restoration*. Image fusion [20], [21], [22], [23] and color transfer [24] are performed to restore a high quality haze-free image.

In Fig. 3, two typical nighttime haze image examples are used to illustrate the dehazing process in detail, where Fig. 3 (a) is a color-shift nighttime haze image, and Fig. 3 (b) is a normal nighttime haze image.

A. Atmospheric Light Decomposition

Images captured during nighttime may present a color-bias phenomenon (as shown in Fig. 3 (a)). In order to deal with the complex situations, we use the shades-of-gray algorithm [25] [26] to correct the color of the input nighttime image in this paper. This algorithm assumes that the Minkowski norm of a scene reflection component is achromatic and the order of the Minkowski norm is between 1 and infinity.

In our work, to roughly depict the non-uniform illumination property in nighttime, we compute the color of the input nighttime haze image corresponding to three different orders to balance the smoothing effect and detailed information, where the order values N are defined as:

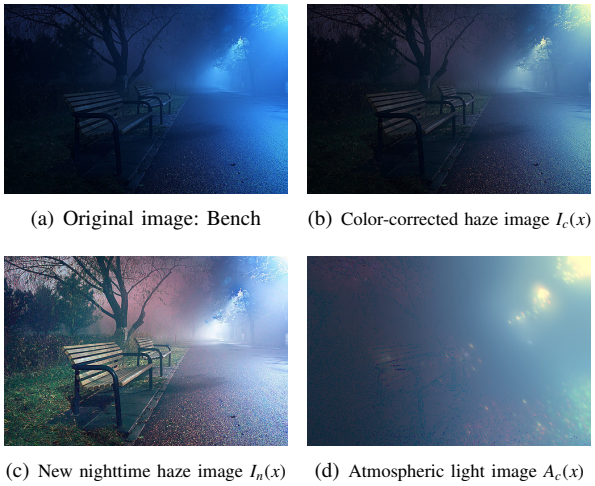

(a) Original image: Bench (b) Color-corrected haze image $I_c(x)$

(c) New nighttime haze image $I_n(x)$ (d) Atmospheric light image $A_c(x)$

Fig. 4: The process of decomposing an atmospheric light image.

$$N = \lfloor \min(m, n)/k \rfloor, \quad \text{for} \quad k \in \{10, 20, 40\}, \tag{3}$$

where m and n are the length and width of input nighttime image respectively, $\min(\cdot)$ means to take a minimum value, $\lfloor x \rfloor$ is the floor function that outputs the greatest integer less than or equal to the real number x, and the values of k correspond to the large, medium and small sizes of N.

Next, three correction images $I_1(x)$, $I_2(x)$ and $I_3(x)$ can be computed by the shades-of-gray algorithm [25] [26] with the above three different order values N.

Considering the global color feature of shades-of-gray algorithm, the color-corrected haze image $I_c(x)$ is obtained by fusing the three correction images as:

$$I_c(x) = r_1(x) \times I_1(x) + r_2(x) \times I_2(x) + r_3(x) \times I_3(x), \tag{4}$$

where

$$\begin{cases} r_1(x) = I_1(x)/(I_1(x) + I_2(x) + I_3(x) + \epsilon) \\ r_2(x) = I_2(x)/(I_1(x) + I_2(x) + I_3(x) + \epsilon) \\ r_3(x) = I_3(x)/(I_1(x) + I_2(x) + I_3(x) + \epsilon), \end{cases} \tag{5}$$

Here, ϵ is an infinitesimal, to avoid division by zero.

Referring to Eq. 2, the color-corrected haze image $I_c(x)$ in Eq. 4 can be represented using its color-corrected components as:

$$\begin{aligned} I_c(x) &= J_c(x)t_c(x) + A_c(x)[1 - t_c(x)] \\ &= A_c(x)\rho_c(x)t_c(x) + A_c(x)[1 - t_c(x)] \\ &= A_c(x)[\rho_c(x)t_c(x) + 1 - t_c(x)]. \end{aligned} \tag{6}$$

Based on the Retinex theory [27], from Eq. 6, a new nighttime haze image $I_{nw}(x)$ can be computed as:

$$I_{nw}(x) = R[I_c(x)] = \rho_c(x)t_c(x) + 1 - t_c(x), \tag{7}$$

where R represents the Retinex operation.

It is well known that the max value of $A_c(x)$ is not greater than 1. Thus, from Eqs. 6 and 7, the values of $I_{nw}(x)$ are not less than the corresponding values in $I_c(x)$. Thus, $I_{nw}(x)$ can be rewritten as $I_n(x)$:

$$I_n(x) = \max(I_{nw}(x), I_c(x)), \tag{8}$$

where $\max(\cdot)$ means to take a maximum value. At the same time, from Eqs. 6 and 8, the atmospheric light image $A_c(x)$ can be obtained as:

$$A_c(x) = I_c(x)/(I_n(x) + \epsilon). \tag{9}$$

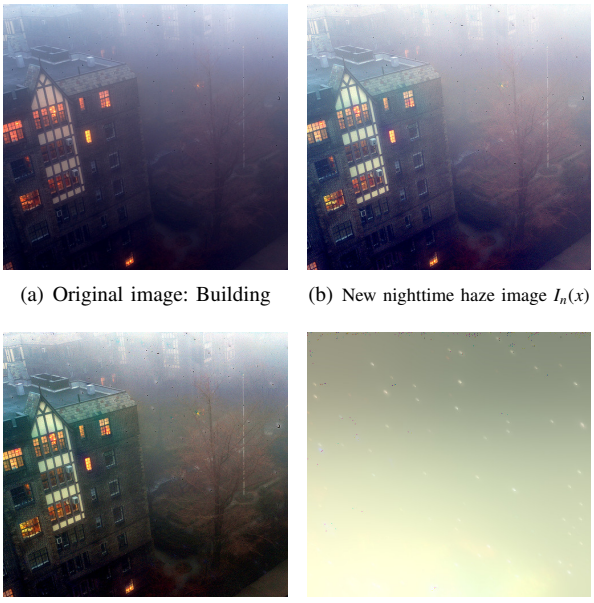

(a) Original image: Building (b) New nighttime haze image $I_n(x)$

(c) Initial haze-free image $J_{init}(x)$ (d) Coarse transmission map $t_{coar}(x)$

Fig. 5: The process of decomposing a coarse transmission map.

In Eq. 7, the Retinex algorithm comes from [27], and it is called as Frankle-McCann Retinex. In this algorithm, there is a parameter '*nIterations*', which is used to decide the dynamic range of compression. To balance the computation complexity and accuracy of the estimation, the value of *nIterations* is set to 8 in this paper. In Section IV-C, ablation study about the parameter '*nIterations*' is presented in Fig. 13.

Fig. 4 illustrates the process of decomposing an atmospheric light image using an exemplar benchmark image 'Bench'. From Eqs. 6, 7 and 8 and Fig. 4 (c), a new nighttime haze image $I_n(x)$ looks like a daytime haze image with white balance. Under this circumstance, the dark channel prior is suitable to deal with $I_n(x)$ and $\rho_c(x)$ is regarded as a haze-free image. As can be seen from Fig. 4 (d), $A_c(x)$ is not constant in numerical value and varies by location, and has a color similar to that of color-corrected haze image, which will be used in Section III-C.

B. Transmission Map Estimation

As proven in [11], from Eqs. 7 and 8, we can get

$$1 - I_n(x) = [1 - \rho_c(x)]t_c(x), \tag{10}$$

where $t_c(x)$ only depends on the scattering coefficient β and scene depth $d(x)$ from the definition of transmission map, which is no greater than 1. And the three color channel images of $t_c(x)$ are the same because of same β and $d(x)$. So, similar to Eq. 7, the Retinex algorithm [27] is used to get the negative haze-free image $J_{ne}(x)$ as:

$$J_{ne}(x) = R[1 - I_n(x)] = 1 - \rho_c(x). \tag{11}$$

Referring to Eq. 8, $J_{ne}(x)$ can be rewritten as:

$$J_{ne}(x) = \max(1 - I_n(x), J_{ne}(x)). \tag{12}$$

Then, from Eqs. 11 and 12, an initial haze-free image $J_{init}(x)$ can be defined as:

$$J_{init}(x) = 1 - J_{ne}(x). \tag{13}$$

Meanwhile, from Eqs. 10 and 12, a coarse transmission map $t_{coar}(x)$ can be obtained as:

$$t_{coar}(x) = (1 - I_n(x))/(J_{ne}(x) + \epsilon). \tag{14}$$

As shown in Fig. 5 (c), the initial haze-free image $J_{init}(x)$ has already achieved a good dehazing effect, but the overall brightness of $J_{init}(x)$ is rather bright especially in the area of distant buildings, which will be addressed next.

After the atmospheric light image $A_c(x)$ is decomposed and the initial haze-free image $J_{init}(x)$ is estimated, in the following content, the dark channel prior using Taylor series expansion is adopted to obtain the haze-free image.

First, a minimum operation is applied on both sides of Eq. 7 and a dark channel image of $I_n(x)$, denoted as $I^{dark}(x)$, is expressed as:

$$\begin{aligned} I^{dark}(x) &= \min_{C\in\{R,G,B\}} I_n^C(x) \\ &= \min_{C\in\{R,G,B\}} [\rho_c^C(x)t_c^C(x) + 1 - t_c^C(x)] \\ &= \rho_c^{dark}(x)t_{c_{sc}}(x) + 1 - t_{c_{sc}}(x), \end{aligned} \tag{15}$$

where C is a color channel, $\min_{C\in\{R,G,B\}}$ takes the minimum value of the RGB three-channel gray value for each pixel. $I^{dark}(x)$ and $\rho_c^{dark}(x)$ represent the dark channel images of $I_n(x)$ and $\rho_c(x)$, respectively. $t_{c_{sc}}(x)$ is any a color channel image of $t_c(x)$.

In order to eliminate the influence of bright objects, *e.g.*, artificial light sources, minimum filtering is performed on $I^{dark}(x)$. The domain size S of minimum filtering has the same values as N to obtain the three filtered images $\hat{I}_1^{dark}(x)$, $\hat{I}_2^{dark}(x)$ and $\hat{I}_3^{dark}(x)$.

Similar to Eqs. 4, 5 and 6, $\hat{I}_1^{dark}(x)$, $\hat{I}_2^{dark}(x)$ and $\hat{I}_3^{dark}(x)$ are used to obtain the final minimum filtered image $\hat{I}^{dark}(x)$ with the same process, and Eq. 15 can be rewritten using its minimum-filtered components as:

$$\hat{I}^{dark}(x) = \hat{\rho}_c^{dark}(x)\hat{t}_{c_{sc}}(x) + 1 - \hat{t}_{c_{sc}}(x). \tag{16}$$

Based on the dark channel prior [2], the values of $\hat{\rho}_c^{dark}(x)$ approach to zero. Therefore, it is easy to get a lower-bound transmission map $t_L(x)$ from Eq. 16 as:

$$t_L(x) = 1 - \hat{I}^{dark}(x). \tag{17}$$

From Eq. 16, $\hat{t}_{c_{sc}}(x)$ can be derived as:

$$\hat{t}_{c_{sc}}(x) = \frac{1 - \hat{I}^{dark}(x)}{1 - \hat{\rho}_c^{dark}(x)} = 1 - \frac{\hat{I}^{dark}(x) - \hat{\rho}_c^{dark}(x)}{1 - \hat{\rho}_c^{dark}(x)}. \tag{18}$$

According to Eq. 18, a new function with the variable $\hat{\rho}_c^{dark}(x)$ can be defined as:

$$f(\hat{\rho}_c^{dark}(x)) = \frac{\hat{I}^{dark}(x) - \hat{\rho}_c^{dark}(x)}{1 - \hat{\rho}_c^{dark}(x)}, \tag{19}$$

where $\hat{I}^{dark}(x)$ is considered as a known quantity from Eqs. 2, 6, 7, 8, 15 and 16.

Here, the first-order Taylor expansion is adopted to deal with $f(\hat{\rho}_c^{dark}(x))$ as:

$$\begin{aligned} f(\hat{\rho}_c^{dark}(x)) &= f(\hat{\rho}_c^{dark}(x_0)) + f'(\hat{\rho}_c^{dark}(x_0))(\hat{\rho}_c^{dark}(x) - \hat{\rho}_c^{dark}(x_0)) \\ &= f(\hat{\rho}_c^{dark}(x_0)) + \left[\frac{\hat{I}^{dark}(x) - \hat{\rho}_c^{dark}(x_0)}{(1 - \hat{\rho}_c^{dark}(x_0))^2} - \frac{1}{1 - \hat{\rho}_c^{dark}(x_0)}\right] \\ &\bullet(\hat{\rho}_c^{dark}(x) - \hat{\rho}_c^{dark}(x_0)), \end{aligned} \tag{20}$$

where $\hat{\rho}_c^{dark}(x_0)$ is an expansion point.

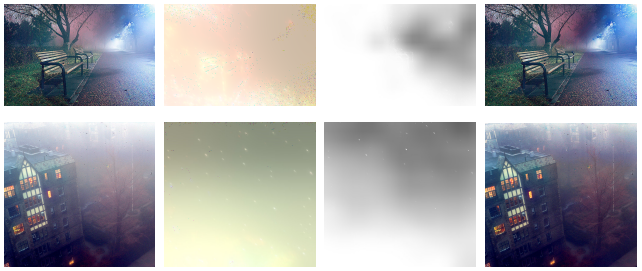

(a) $I_n(x)$ (b) $t_{coar}(x)$ (c) $t(x)$ (d) $J_{pote}(x)$

Fig. 6: The process of estimating the transmission maps to obtain the potential haze-free images. (a) New nighttime haze images $I_n(x)$; (b) Coarse transmission maps $t_{coar}(x)$; (c) Transmission maps $t(x)$; (d) Potential haze-free images $J_{pote}(x)$.

Considering that our target focuses on dehazing nighttime images, from Eqs. 18, 19 and 20, when the values of $\hat{\rho}_c^{dark}(x_0)$ are approaching to zero, a new representation of $\hat{t}_{c_{sc}}(x)$ can be obtained using the dark channel prior [2] as:

$$\begin{aligned}\hat{t}_{c_{sc}}(x) &= 1 - \left[\hat{I}^{dark}(x) - \hat{\rho}_c^{dark}(x) + \hat{I}^{dark}(x) \times \hat{\rho}_c^{dark}(x)\right] \\ &= \left[1 - \hat{I}^{dark}(x)\right] \times \left[1 + \hat{\rho}_c^{dark}(x)\right] \\ &\leqslant \left[1 - \hat{I}^{dark}(x)\right] \times \left[1 + \hat{I}^{dark}(x)\right] = 1 - \left[\hat{I}^{dark}(x)\right]^2.\end{aligned} \tag{21}$$

Note that, $0 \leq \hat{t}_{c_{sc}}(x) \leq 1$ and $\hat{I}^{dark}(x) \geq \hat{\rho}_c^{dark}(x)$ derived from Eq. 18 are applied in Eq. 21.

Then, from Eq. 21, an upper-bound transmission map $t_U(x)$ can be computed as:

$$t_U(x) = 1 - \left[\hat{I}^{dark}(x)\right]^2. \tag{22}$$

Therefore, from Eqs. 17 and 22, any one color channel image $t_{UL}(x)$ of the transmission map $t(x)$ can be obtained by:

$$t_{UL}(x) = \omega \times t_U(x) + (1 - \omega) \times t_L(x), \tag{23}$$

where

$$\omega = \frac{t_U(x) - t_L(x)}{t_L(x) + \epsilon}. \tag{24}$$

From Eq. 15, the values of $\rho_c^{dark}(x)$ are not less than zero. So, another lower-bound transmission map $t_l(x)$ is defined as:

$$t_l(x) = 1 - I^{dark}(x). \tag{25}$$

Combining Eqs. 14 and 25, $t_{coar}(x)$ is updated by:

$$t_{coar}^C(x) = \max\{t_{coar}^C(x), t_l(x)\}, \quad \text{for} \quad C \in \{R, G, B\}. \tag{26}$$

Then, three color channel images of $t_{coar}(x)$ are introduced to use the procedures in Eqs. 4 and 5 for obtaining an edge-guided image $I_g(x)$, which is adopted to optimize $t_{UL}(x)$ in Eq. 23 with bilateral filtering [28].

So, the final transmission map $t(x)$ can be got using the optimized $t_{UL}(x)$. And according to Eqs. 7 and 8, a potential haze-free image $J_{pote}(x)$ can be obtained by:

$$J_{pote}(x) = \frac{I_n(x) - \theta \times (1 - t(x))}{t(x) + \epsilon}, \tag{27}$$

where θ is a regulation parameter affecting the degree of dehazing, and it is empirically set to 1.05.

We should note that there are some transmission map expressions in the process of obtaining $t(x)$, such as $\hat{t}_{c_{sc}}(x)$, $t_{coar}(x)$, *etc.*. In our paper, the dark channel prior [2] is used to achieve $\hat{t}_{c_{sc}}(x)$ and $t_L(x)$ from Eq. 16. Then, we introduce Taylor series expansion to obtain the upper-bound transmission map $t_U(x)$ from $\hat{t}_{c_{sc}}(x)$. Subsequently, pixel fusion is adopted to get $t_{UL}(x)$. From Eq. 14, we use the Retinex theory to get $t_{coar}(x)$, which is used to obtain the edge-guided image $I_g(x)$. For better edge preservation, $I_g(x)$ is utilized to filter $t_{UL}(x)$ with joint bilateral filtering to obtain the final transmission map $t(x)$. Therefore, $\hat{t}_{c_{sc}}(x)$, $t_{coar}(x)$ and other transmission map expressions are the required inputs in the process of obtaining $t(x)$.

As shown in Fig. 6 (d), thanks to the accurate transmission map, the method of potential haze-free image estimation achieves good dehazing results, and it is referred to as 'RDT-Source' method in our experiments.

(a) $J_{fuse}(x)$ (b) $J_{refe}(x)$ (c) $J_{ct}(x)$ (d) $J(x)$

Fig. 7: The process of image fusion to restore a nighttime haze-free image using the image 'Building'. (a) Fused haze-free image $J_{fuse}(x)$; (b) Nighttime haze-free reference image $J_{refe}(x)$; (c) Nighttime color transfer image $J_{ct}(x)$; (d) Nighttime haze-free image $J(x)$.

(a) Original image: Bench (b) $J_{pote}(x)$ (c) $J(x)$

Fig. 8: The result of nighttime haze-free image. (a) Original image: Bench; (b) Potential haze-free image $J_{pote}(x)$; (c) Nighttime haze-free image $J(x)$.

C. Image Fusion and Restoration

From Figs. 5 (c) and 6 (d), the haze-free images are brighter compared with the corresponding nighttime haze images. It may be related to the fact that the Retinex algorithm regularizes the dynamic range of an input image. However, we find the main reason is that the non-uniform atmospheric light map $A_c(x)$ of a nighttime haze scene has not been taken into account. That is to say, referring to Eqs. 6 and 9, $J_{pote}(x)$ deduced from Eqs. 7 and 8 does not consider the influence of $A_c(x)$. As shown in Fig. 2, we can apply the image fusion algorithm [20], [29] to fuse the atmospheric light map $A_c(x)$ with the estimated haze-free image obtained from $J_{init}(x)$ and $J_{pote}(x)$ to solve the problem, and the image color is then further adjusted with a color transferring algorithm [24] as the final output.

First, the image fusion algorithm [20] [30] is utilized to fuse $J_{init}(x)$ in Eq. 13 and $J_{pote}(x)$ in Eq. 27 to obtain a fused image $J_{fuse}(x)$ (shown in Fig. 7 (a)).

Next, using the non-uniform atmospheric light map $A_c(x)$, a nighttime haze-free reference image $J_{refe}(x)$ is defined by:

$$J_{refe}(x) = J_{fuse}(x) \times A_c(x). \tag{28}$$

Note that, $J_{refe}(x)$ (shown in Fig. 7 (b)) is only regarded as the reference color image.

Algorithm 1 Algorithm flow of restoring a nighttime image.

Input: Nighttime haze image, $I(x)$; Nighttime haze imaging model, $I(x) = J(x)t(x) + A(x)[1 - t(x)]$.
Output: Recovered image, $J(x)$.

Using shades-of-gray algorithm and Retinex theory to obtain an atmospheric light image $A_c(x)$ in Eq. 9;
if Dark Channel Prior is satisfied **then**
  $t_L(x) = 1 - \hat{I}^{dark}(x)$ in Eq. 17;
  while First-order Taylor expansion is adopted **do**
    $t_U(x) = 1 - \left[\hat{I}^{dark}(x)\right]^2$ in Eq. 22;
  end while
  Using pixel-level fusion method and bilateral filtering algorithm to get the final transmission map $t(x)$;
end if
Using $A_c(x)$ and $t(x)$ with image fusion and color transfer algorithms to obtain $J(x)$;
return $J(x)$.

Then, in order to properly retain the characteristics of nighttime image while removing haze, the color transfer algorithm shown in [24] [31] is used to transfer the color characteristics of $J_{refe}(x)$ to $J_{pote}(x)$. In other word, $J_{pote}(x)$ borrows the color characteristics from $J_{refe}(x)$ to obtain a color transfer image $J_{ct}(x)$ (shown in Fig. 7 (c)). Finally, a nighttime haze-free image $J(x)$ (shown in Fig. 7 (d)) can be obtained by:

$$J(x) = J_{ct}(x)/V(x), \tag{29}$$

where $V(x)$ is the maximum pixel value in $J_{ct}(x)$, which is used to normalize the image.

From Figs. 7 (d) and 8 (c), by image fusion and color transfer, the proposed method is able to correct color distortion and enhance visibility, and it is referred to as 'RDT-Target' method in this paper.

D. Algorithm Flow

By combining the aforementioned three parts, Algorithm 1 summarizes the steps to obtain a nighttime haze-free image.

IV. Experiments and Results

To demonstrate the performance of the proposed method, a series of experiments are conducted to compare with several state-of-the-art methods [2], [13], [14], [15], [16], [17] on synthetic and natural haze images. All of the state-of-the-art results are obtained using the original codes provided by the corresponding authors on their homepages or GitHub webpages. We evaluate and compare the dehazing results in both objective and subjective ways on the same sets of testing images.

Note that, from Section III-B and III-C, our proposed method is referred as the RDT-Source method and RDT-Target method in this paper, which are used to get a potential haze-free image and the final nighttime haze-free image, respectively. What is more, there are no parameters that need to be modified or adjusted for images of different sources in our method. In this paper, all experiments are conducted on a laptop with a 2.5 GHz Intel Core 2 Processor.

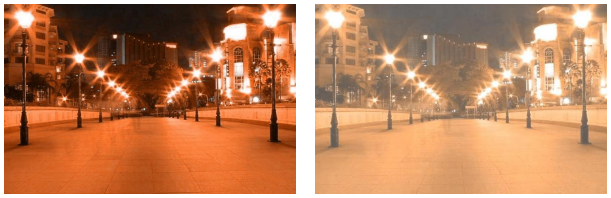

(a) Ground truth: Street Lamp (b) Synthetic image: Street Lamp

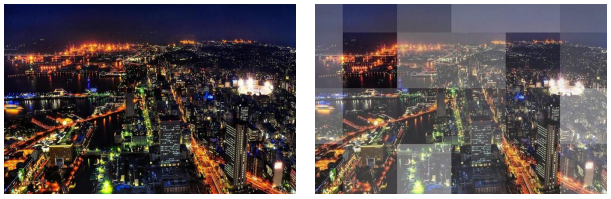

(c) Ground truth: City Light (d) Synthetic image: City Light

Fig. 9: The ground truth and synthetic images of two exemplar images. First row: the Street Lamp image (a) added with uniform haze (b). Second row: the City Light image (c) added with variable haze (d).

TABLE I: Quantitative assessment of two exemplar synthetic nighttime haze images using the evaluation methods of PSNR, SSIM and CIEDE2000. First and second best results are highlighted in color.

Name	Street Lamp			City Light		
	PSNR	SSIM	CIEDE2000	PSNR	SSIM	CIEDE2000
Li *et al.* [15]	17.232	0.351	22.320	7.549	0.061	36.536
Zhang *et al.* [13]	13.375	0.367	22.944	11.314	0.116	29.620
Liao *et al.* [16]	23.204	0.686	10.758	13.104	0.196	24.778
Yang *et al.* [17]	19.801	0.463	21.137	6.747	0.080	37.974
RDT-Source	18.165	0.512	15.370	11.037	0.120	30.169
RDT-Target	18.138	0.431	15.890	11.308	0.124	29.190

TABLE II: The average PSNR, SSIM and CIEDE2000 of 1000 random synthetic nighttime image dehazing results from datasets NightHaze-1 and NightHaze-2 [16]. First and second best results are highlighted in color.

Name	Li *et al.*	Zhang *et al.*	Liao *et al.*	Yang *et al.*	Our Method	
					RDT-Source	RDT-Target
PSNR	11.600	13.133	13.931	11.904	13.308	13.188
SSIM	0.167	0.184	0.209	0.189	0.194	0.199
CIEDE2000	21.741	20.638	18.895	21.372	19.503	19.472

A. Dehazing Results on Synthetic Nighttime Haze Images

We first verify and quantitatively compare the dehazing effect on synthetic nighttime haze images. Two hazy image datasets NightHaze-1 and NightHaze-2 [16] are used in this paper. The collected nighttime images in NightHaze-1 [16] are globally added with haze of uniform density. NightHaze-2 [16], the collected images are added into small patches at a certain probability, with some patches containing no haze. As shown in Fig. 9, the first image called 'Street Lamp' (see Fig. 9(b)) is from NightHaze-1 [16], while the second image called 'City Light' (see Fig. 9(d)) is from NightHaze-2 [16].

The dehazing results on the two synthetic haze images shown in Fig. 9 obtained with several benchmark methods are shown in Fig. 10 (b)-(g), corresponding to the dehazing results obtained using Li *et al.*'s method [15], Zhang *et al.*'s method [13], Liao *et al.*'s method [16], Yang *et al.*'s method [17], the proposed RDT-Source method and the proposed RDT-Target method, respectively. Among these methods, Liao *et al.*'s method [16] is a learning-based technique and the other methods rely on explicit priors or hypotheses. Some close-up views of the dehazing results are shown in the

(a) Haze images (b) Li *et al.* (c) Zhang *et al.* (d) Liao *et al.* (e) Yang *et al.* (f) RDT-Source (g) RDT-Target

Fig. 10: Dehazing results on the two exemplar synthetic nighttime haze images shown in Fig. 9 by comparing with state-of-the-art results. (a) Nighttime haze images; (b) ~ (g) Results of Li *et al.* [15], Zhang *et al.* [13], Liao *et al.* [16], Yang *et al.* [17], our RDT-Source and RDT-Target.

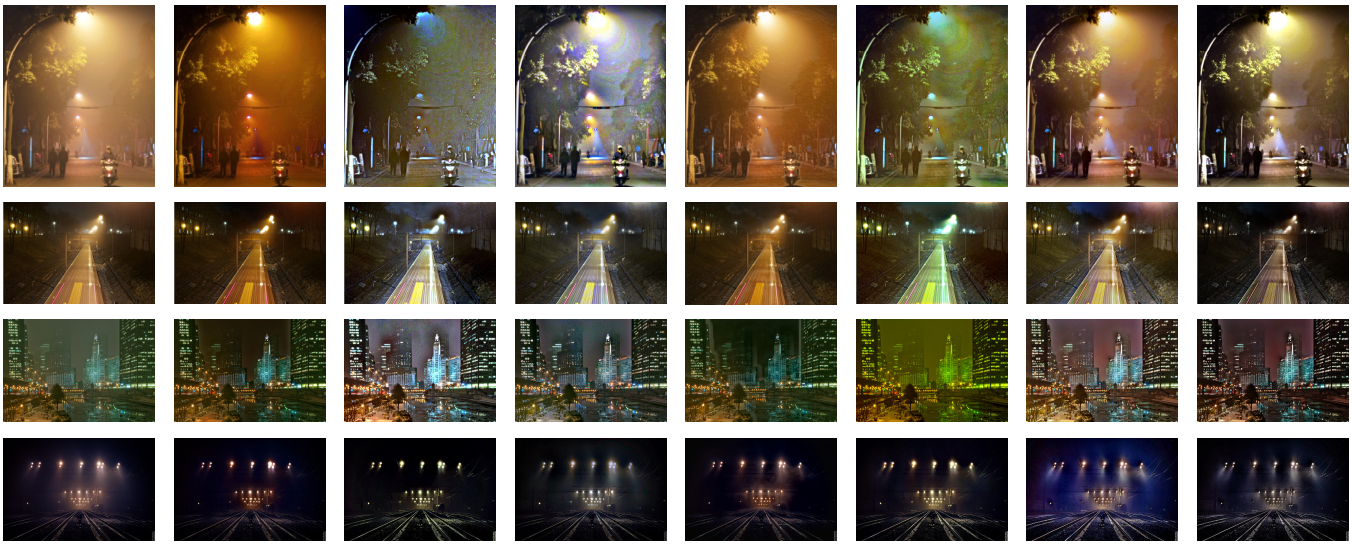

(a) Haze images (b) He *et al.* (c) Li *et al.* (d) Zhang *et al.* (e) Liao *et al.* (f) Yang *et al.* (g) RDT-Source (h) RDT-Target

Fig. 11: Qualitative results on natural nighttime haze images by comparing with state-of-the-art results. (a) Nighttime haze images; (b) ~ (h) Results of He *et al.* [2], Li *et al.* [15], Zhang *et al.* [13], Liao *et al.* [16], Yang *et al.* [17], our RDT-Source and RDT-Target.

even rows. Peak Signal-to-Noise Ratio (PSNR) [32], Structural Similarity (SSIM) [33] and CIEDE2000 [34] are adopted as the quantitative assessment indexes to quantitatively measure the dehazing effects, and the results are shown in Table I. In this table, the numbers in red indicate the best results and the numbers in green represent the second best results.

From Table I, Liao *et al.*'s method [16] seems to have the best results in terms of numbers. However, from Fig. 9 (a), (c) and Fig. 10 (d), the dehazing effects of Liao *et al.*'s method are not obvious and appear a little blurry compared with the other methods. As can be seen from the first two rows of Fig. 10, the dehazing results obtained by using Zhang *et al.*'s method [13] contain obvious color distortion. Li *et al.*'s method [15] can effectively remove haze effects, but it is easy to over-enhance local areas and over-amplify colors. Yang *et al.*'s method [17] is comparable to our RDT-Source and RDT-Target methods in dehazing performance, but it appears a little worse in color fidelity. From the last two rows of Fig. 10, the methods of Li *et al.* [15] and Yang *et al.* [17] present color shifts in the sky areas and some parts of restored images seem to be over-enhanced. Compared with [13], the proposed RDT-Source and RDT-Target methods obtain competitive results and have better color fidelity in sky areas. In general, the results of the proposed RDT-Source and RDT-Target methods are close to the ground truth and have better clarity, contrast and color fidelity.

To illustrate, 1000 typical synthetic nighttime images from datasets NightHaze-1 and NightHaze-2 [16] are selected for quantitative comparison. The quantitative results of comparative methods are displayed in Table II. From the average values

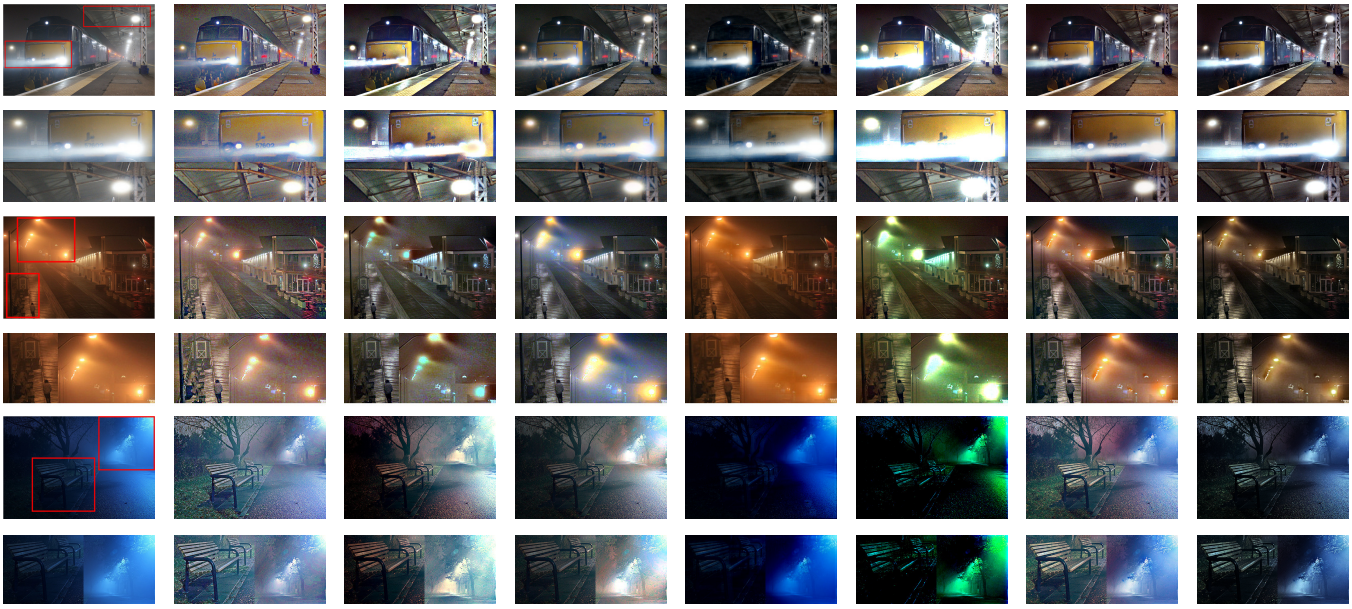

(a) Haze images (b) Zhang *et al.* (c) Li *et al.* (d) Zhang *et al.* (e) Liao *et al.* (f) Yang *et al.* (g) RDT-Source (h) RDT-Target

Fig. 12: Qualitative results on natural nighttime haze images by comparing with state-of-the-art results. (a) Nighttime haze images; (b) ∼ (h) Results of Zhang *et al.* [14], Li *et al.* [15], Zhang *et al.* [13], Liao *et al.* [16], Yang *et al.* [17], our RDT-Source and RDT-Target.

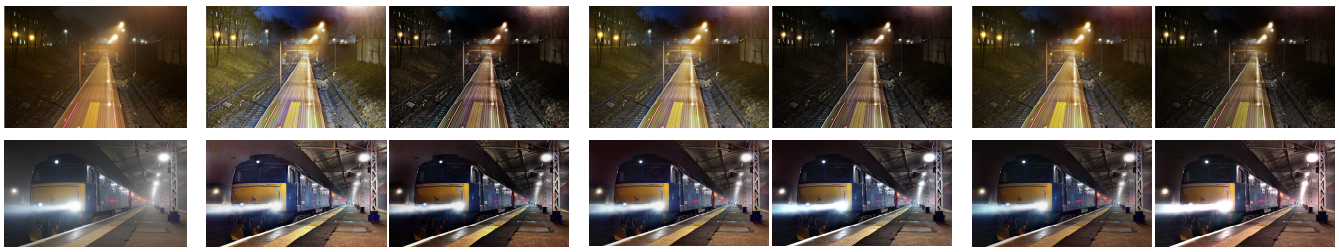

(a) Original images (b) *nIterations*=4 (c) *nIterations*=8 (d) *nIterations*=16

Fig. 13: Retinex algorithm used in nighttime haze images dehazing with three different values of *nIterations*. (a) Original images: Treno and Train (from up to down); (b), (c) and (d) dealt with our proposed method (*i.e.*, our RDT-Source and RDT-Target methods from left to right in each image) using three different values.

of PSNR, SSIM and CIEDE2000, our results are comparable to Liao *et al.*'s method [16] and outperform other methods. Similar to the analyses of Fig. 10 and Table I, our method can obtain better nighttime image dehazing effect.

B. Qualitative Results on Natural Nighttime Haze Images

To further assess the effectiveness of the proposed method, several natural nighttime haze images (shown in Figs. 11 (a) and 12 (a)) are used. In Fig. 12, some close-up views of the dehazing results are shown in the even rows. The compared dehazing methods of He *et al.* [2], Zhang *et al.* [14], Li *et al.* [15], Zhang *et al.* [13], Liao *et al.* [16] and Yang *et al.* [17] are adopted to complete the qualitative assessment. Among these methods, He *et al.*'s method [2] is a daytime dehazing technique and the other methods are the nighttime dehazing techniques. We should note that, as described in [35] and [2], keeping an amount of haze can ensure the authenticity of dehazed image.

Fig. 11 shows that methods of He *et al.* [2] and Liao *et al.* [16] tend to fail in dehazing performance (see the first image in Fig. 11 (b) and (e)). The brightness of dehazing results in [2] (see the second and fourth images in Fig. 11 (b)) appear a little dark and the dehazing results in [16] (see the third and fourth images in Fig. 11 (e)) present a certain halo effect. Li *et al.*'s method [15] is prone to generate color fringing artifacts around the strong edges (see the second image in Fig. 11 (c)). Zhang *et al.*'s method [13] cannot deal well with the strong light of artificial light sources (see the first image in Fig. 11 (d)). Yang *et al.*'s method [17] cannot handle the color distortion very well (see the first and third images in Fig. 11 (f)). From Fig. 11 (h), the proposed RDT-Target method can correct color distortion and produce favorable results.

Fig. 12 reveals that the method of Liao *et al.* [16] tends to leave a lot of haze in the results (see the third and fourth images in Fig. 12 (e)), Yang *et al.*'s method [17] is easy to produce color distortion (see the fifth and sixth images in Fig. 12 (f)), the methods of Zhang *et al.* [14] and Li *et al.* [15] produce over-enhancement in the local areas resulting in noise amplification (see the first and second images in Fig. 12 (b) and (c)), and Zhang *et al.*'s method [13] is difficult to cope with the light source glow (see the third and fourth images

(a) Original images (b) k=10 (c) k=20 (d) k=40 (e) k=80 (f) $k \in \{10,20,40\}$

Fig. 14: Color correction and minimum filtering of nighttime haze images with five different values of k. First row: the color corrected images. Second row: the potential haze-free images.

TABLE III: The average scores of Detail Recognition (DR), Color Fidelity (CF), Image Authenticity (IA) and Overall Effect (OE) in the user study. First and second best results are highlighted in color.

Name	He *et al.*	Li *et al.*	Zhang *et al.*	Liao *et al.*	Yang *et al.*	Our Method	
						RDT-Source	RDT-Target
DR	2.852	3.914	3.853	2.771	3.327	4.150	3.893
CF	3.560	2.432	3.216	3.263	2.550	3.772	3.934
IA	3.096	3.312	3.380	3.052	2.944	3.672	4.085
OE	3.155	3.437	3.535	3.173	2.966	3.793	3.964

TABLE IV: Comparison of the computation time (in seconds) between our proposed method using Retinex algorithm with three different values of *nIterations* and the other two methods.

Name	Size	Our method				Li *et al.*	Yang *et al.*
		nIterations	T1/sec	T2/sec	T/sec	T/sec	T/sec
Treno	382 × 576 × 3	4	1.854	4.357	7.326	15.317	8.396
		8	**3.294**	**8.250**	**11.257**		
		16	6.048	15.732	18.710		
Train	446 × 752 × 3	4	2.936	6.833	11.997	47.924	30.195
		8	**5.006**	**12.685**	**17.639**		
		16	9.508	24.518	29.437		

in Fig. 12 (d)). Overall, the proposed RDT-Target method can obtain realistic colors while removing haze better as shown in Fig. 12 (h).

Further, the similar as described in [36], we conduct a user study with 40 participants to compare results. Firstly, 80 test images are selected from cited papers and Flickr. Then, we dehaze each test image using our method and methods of He *et al.* [2], Li *et al.* [15], Zhang *et al.* [13], Liao *et al.* [16] and Yang *et al.* [17]. For each result, the participants are asked to give a score for each of the four aspects, *i.e.*, Detail Recognition (DR), Color Fidelity (CF), Image Authenticity (IA) and Overall Effect (OE). The value of score is measured to 2 decimal places from 1.00 (worst) to 5.00 (best), and the average score is computed to 3 decimal places. As shown in Table III, one can see that our results are more preferred by human subjects, where our method receives a higher average score compared to the others.

C. Algorithm Characteristics Analysis

From the above detailed description of the proposed method in Section III, there are three parameters in our algorithm, *i.e.*, the iteration number *nIterations* of Retinex algorithm, the order value N of Minkowski norm and the domain size S of minimum filtering. From the description in Section III-A and III-B and Eq. 3, N and S have the same values and depend on the values of k. To highlight the characteristics of the proposed method, we discuss the impact of the three parameters *nIterations*, N and S on the effectiveness of our proposed method.

As shown in Fig. 13 (b), (c) and (d) (see the first row of the figure), with the increasing number of *nIterations*, the overall brightness of the haze-free images drops, but it looks more natural. Compared with Fig. 13 (d) in the first row of the figure, Fig. 13 (c) has a better visual effect and the restored color of Fig. 13 (d) is a little dark. From the second row of the figure, Fig. 13 (b) shows a bit over-dehazing and Fig. 13 (d) looks like a little color distortion. In general, Fig. 13 (c) obtains a better dehazing effect.

Table IV describes the computation time used by the Retinex algorithm with three different values of *nIterations* during the process of our proposed method. In Table IV, T1 is the time from the beginning of our algorithm to the end of the first-mentioned Retinex algorithm, T2 computes the time from the beginning of our algorithm to the end of the second-mentioned Retinex algorithm, and T shows the total time of our algorithm. From the values of *nIterations*, T1 and T2 increase almost linearly as *nIterations* increases. Compared with T in numerical value, the proportion of time of T1 or T2 spent in the Retinex algorithm improves with the increase of *nIterations*. Therefore, according to Fig. 13 and Table IV, *nIterations* is set to 8 in our algorithm.

In addition, the methods of [15] and [17] are adopted to compare with our proposed method in term of the computation time, which are all implemented using Matlab codes. In [13] and [14], the authors provide the OpenCV codes. And Python code is adopted in [16]. It can be seen from Table IV that our proposed RDT-Target method (see the results in Fig. 13 (c)) takes 11.257 seconds and 17.639 seconds to deal with the images using default parameter settings. And Li *et al.*'s method [15] (see the results in second row of Fig. 11 (c) and first row of Fig. 12 (c)) spends 15.317 seconds and 47.924 seconds, as well as 8.396 seconds and 30.195 seconds with Yang *et al.*'s method [17] (see the results in second row of Fig. 11 (f) and first row of Fig. 12 (f)). It is clear to see, with the increasing number of image size, the performance of our method will be faster and more stable compared with the methods of Li *et al.* [15] and Yang *et al.* [17].

As can be seen from Fig. 14, with the increasing number of k, the color correction effects gradually become worse and the degrees of haze removal are increasingly enhanced. When k takes the values of 10, 20 and 40 for image fusion

(a) Daytime haze images (b) He *et al.* [2] (c) Cai *et al.* [37] (d) RDT-Source (e) RDT-Target

Fig. 15: Qualitative results on natural daytime haze images by comparing with state-of-the-art results. (a) Daytime haze images; (b) ~ (e) Results of He *et al.* [2], Cai *et al.* [37], our RDT-Source and RDT-Target.

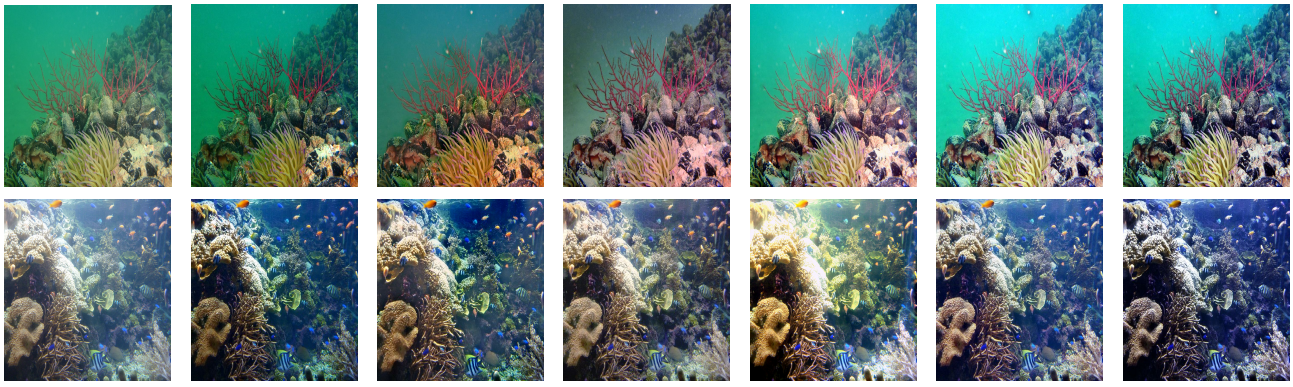

(a) Original (b) He *et al.* (c) Chiang *et al.* (d) Ancuti *et al.* (e) Akkaynak *et al.* (f) RDT-Source (g) RDT-Target

Fig. 16: Qualitative results on underwater images by comparing with state-of-the-art results. (a) Original; (b) ~ (g) Results of He *et al.* [2], Chiang *et al.* [38], Ancuti *et al.* [39], Akkaynak *et al.* [40], our RDT-Source and RDT-Target.

(shown in Fig. 14 (f)), the images using color correction and minimum filtering show a trade-off among color fidelity maintenance, clarity improvement and contrast enhancement. In our algorithm, k takes the values of 10, 20 and 40.

From the above analyses, we do not need to adjust the parameters of proposed algorithm.

D. Extension to More Applications

Although our algorithm is designed for nighttime image dehazing, we can extend it to daytime and underwater dehazing.

In Fig. 15, the methods of He *et al.* [2] and Cai *et al.* [37] are designed for daytime image dehazing, and Cai *et al.*'s method [37] is a deep learning approach. From the results of Fig. 15, our proposed method can also obtain high clarity and color fidelity. As shown in Fig. 16, we give two examples of underwater image dehazing. Ignoring the forward scattering component, the simplified underwater optical model [41] has similar formulation with haze imaging model [42]. The methods of Chiang *et al.* [38], Ancuti *et al.* [39] and Akkaynak *et al.* [40] are designed for underwater image enhancement, and Akkaynak *et al.*'s method [40] is also a deep learning-based approach. From the first row of images in Fig. 16, one can see that results of He *et al.* [2], Chiang *et al.* [38] and Ancuti *et al.* [39] tend to appear a little dark, and color over-enhancing is clear in Chiang *et al.*'s result [38]. Holistically speaking, our proposed method achieves image enhancement effect as good as Akkaynak *et al.*'s method [40]. From the second row of images, there are some over-enhanced areas in the results obtained by the methods of Chiang *et al.* [38] and Akkaynak *et al.* [40]. From a visual effect, our enhancement effect is better than He *et al.*'s result [2] and comparable to Ancuti *et al.*'s result [39].

V. Conclusion

In this paper, a novel method of using a Taylor series expansion based on Retinex and dark channel prior has been proposed for nighttime image dehazing. Compared with the state-of-the-art methods, the proposed method can effectively

correct color distortion, improve image clarity and generate more pleasant image details. This work has further exploited the advantages of dark channel prior using the Taylor series expansion for nighttime haze images. In addition, from Table I, more assessment indexes like FADE [43] or CID [44] will be adopted in the future work.

ACKNOWLEDGMENT

The authors would like to thank the authors of compared papers, who provided related images and original codes, and also the anonymous reviewers for their insightful comments and valuable suggestions. The authors gratefully acknowledge financial support from China Scholarship Council.

This work was supported by National Natural Science Foundation of China (No.51879211), Hunan Provincial Natural Science Foundation of China (No.2017JJ3053), Hunan Provincial Key Research and Development Project of China (No.2017GK2204), and Hunan Provincial Science Research Project of China (Nos.17A051).

REFERENCES

[1] W. E. K. Middleton, *Vision through the atmosphere*. University of Toronto Press, 1952.
[2] K. He, J. Sun, and X. Tang, "Single image haze removal using dark channel prior," *IEEE transactions on pattern analysis and machine intelligence*, vol. 33, no. 12, pp. 2341–2353, 2011.
[3] G. Meng, Y. Wang, J. Duan, S. Xiang, and C. Pan, "Efficient image dehazing with boundary constraint and contextual regularization," in *Proceedings of the IEEE international conference on computer vision*, 2013, pp. 617–624.
[4] R. Fattal, "Dehazing using color-lines," *ACM transactions on graphics (TOG)*, vol. 34, no. 1, p. 13, 2014.
[5] J.-B. Wang, N. He, L.-L. Zhang, and K. Lu, "Single image dehazing with a physical model and dark channel prior," *Neurocomputing*, vol. 149, pp. 718–728, 2015.
[6] Q. Zhu, J. Mai, L. Shao *et al.*, "A fast single image haze removal algorithm using color attenuation prior." *IEEE Trans. Image Processing*, vol. 24, no. 11, pp. 3522–3533, 2015.
[7] D. Berman, S. Avidan *et al.*, "Non-local image dehazing," in *Proceedings of the IEEE conference on computer vision and pattern recognition*, 2016, pp. 1674–1682.
[8] Y. Jiang, C. Sun, Y. Zhao, and L. Yang, "Image dehazing using adaptive bi-channel priors on superpixels," *Computer Vision and Image Understanding*, vol. 165, pp. 17–32, 2017.
[9] W. Wang, X. Yuan, X. Wu, and Y. Liu, "Fast image dehazing method based on linear transformation," *IEEE Transactions on Multimedia*, vol. 19, no. 6, pp. 1142–1155, 2017.
[10] M.-Z. Zhu, B.-W. He, and L.-W. Zhang, "Atmospheric light estimation in hazy images based on color-plane model," *Computer Vision and Image Understanding*, vol. 165, pp. 33–42, 2017.
[11] A. Galdran, A. Alvarez-Gila, A. Bria, J. Vazquez-Corral, and M. Bertalmo, "On the duality between retinex and image dehazing," in *Proceedings of the IEEE Conference on Computer Vision and Pattern Recognition*, vol. 3, no. 7, 2018.
[12] W. Ren, J. Pan, H. Zhang, X. Cao, and M.-H. Yang, "Single image dehazing via multi-scale convolutional neural networks with holistic edges," *International Journal of Computer Vision*, vol. 128, no. 1, pp. 240–259, 2020.
[13] J. Zhang, Y. Cao, S. Fang, Y. Kang, and C. Wen Chen, "Fast haze removal for nighttime image using maximum reflectance prior," in *Proceedings of the IEEE Conference on Computer Vision and Pattern Recognition*, 2017, pp. 7418–7426.
[14] J. Zhang, Y. Cao, and Z. Wang, "Nighttime haze removal based on a new imaging model," in *Proceedings of the IEEE International Conference on Image Processing*, 2014, pp. 4557–4561.
[15] Y. Li, R. T. Tan, and M. S. Brown, "Nighttime haze removal with glow and multiple light colors," in *Proceedings of the IEEE International Conference on Computer Vision*, 2015, pp. 226–234.
[16] Y. Liao, Z. Su, X. Liang, and B. Qiu, "Hdp-net: Haze density prediction network for nighttime dehazing," in *Proceedings of the Pacific Rim Conference on Multimedia*. Springer, 2018, pp. 469–480.
[17] M. Yang, J. Liu, and Z. Li, "Superpixel-based single nighttime image haze removal," *IEEE Transactions on Multimedia*, vol. 20, no. 11, pp. 3008–3018, 2018.
[18] Y. Li and M. S. Brown, "Single image layer separation using relative smoothness," in *Proceedings of the IEEE Conference on Computer Vision and Pattern Recognition*, 2014, pp. 2752–2759.
[19] J. Vazquez-Corral and G. D. Finlayson, "Coupled retinex," in *Color and Imaging Conference*, vol. 2019, no. 1. Society for Imaging Science and Technology, 2019, pp. 7–12.
[20] S. Li, X. Kang, and J. Hu, "Image fusion with guided filtering," *IEEE Transactions on Image Processing*, vol. 22, no. 7, pp. 2864–2875, 2013.
[21] A. Galdran, J. Vazquez-Corral, D. Pardo, and M. Bertalmio, "Fusion-based variational image dehazing," *IEEE Signal Processing Letters*, vol. 24, no. 2, pp. 151–155, 2016.
[22] Z. Deng, L. Zhu, X. Hu, C.-W. Fu, X. Xu, Q. Zhang, J. Qin, and P.-A. Heng, "Deep multi-model fusion for single-image dehazing," in *Proceedings of the IEEE International Conference on Computer Vision*, 2019, pp. 2453–2462.
[23] F. Guo, X. Zhao, J. Tang, H. Peng, L. Liu, and B. Zou, "Single image dehazing based on fusion strategy," *Neurocomputing*, vol. 378, pp. 9–23, 2020.
[24] E. Reinhard, M. Adhikhmin, B. Gooch, and P. Shirley, "Color transfer between images," *IEEE Computer graphics and applications*, vol. 21, no. 5, pp. 34–41, 2001.
[25] G. D. Finlayson and E. Trezzi, "Shades of gray and colour constancy." Society for Imaging Science and Technology, 2004, pp. 37–41.
[26] http://colorconstancy.com/.
[27] B. V. Funt, F. Ciurea, and J. J. McCann, "Retinex in matlab," *Journal of electronic imaging*, vol. 13, no. 1, pp. 48–58, 2004.
[28] C. Tomasi and R. Manduchi, "Bilateral filtering for gray and color images," in *Proceedings of the IEEE International Conference on Computer Vision*, 1998, pp. 839–846.
[29] W. Ren, L. Ma, J. Zhang, J. Pan, X. Cao, W. Liu, and M.-H. Yang, "Gated fusion network for single image dehazing," in *Proceedings of the IEEE Conference on Computer Vision and Pattern Recognition*, 2018, pp. 3253–3261.
[30] https://github.com/RRuschel/Image-fusion.
[31] https://github.com/hangong/reinhard_color_transfer.
[32] Q. Huynh-Thu and M. Ghanbari, "Scope of validity of psnr in image/video quality assessment," *Electronics letters*, vol. 44, no. 13, pp. 800–801, 2008.
[33] Z. Wang, A. C. Bovik, H. R. Sheikh, and E. P. Simoncelli, "Image quality assessment: from error visibility to structural similarity," *IEEE transactions on image processing*, vol. 13, no. 4, pp. 600–612, 2004.
[34] G. Sharma, W. Wu, and E. N. Dalal, "The ciede2000 color-difference formula: Implementation notes, supplementary test data, and mathematical observations," *Color Research & Application*, vol. 30, no. 1, pp. 21–30, 2005.
[35] J. Vazquez-Corral, A. Galdran, P. Cyriac, and M. Bertalmío, "A fast image dehazing method that does not introduce color artifacts," *Journal of Real-Time Image Processing*, pp. 1–16, 2018.
[36] R. Wang, Q. Zhang, C.-W. Fu, X. Shen, W.-S. Zheng, and J. Jia, "Underexposed photo enhancement using deep illumination estimation," in *Proceedings of the IEEE Conference on Computer Vision and Pattern Recognition*, 2019, pp. 6849–6857.
[37] B. Cai, X. Xu, K. Jia, C. Qing, and D. Tao, "Dehazenet: An end-to-end system for single image haze removal," *IEEE Transactions on Image Processing*, vol. 25, no. 11, pp. 5187–5198, 2016.
[38] J. Y. Chiang and A. Ying-Ching Chen, "Underwater image enhancement by wavelength compensation and dehazing (wcid)," *IEEE Transactions on Image Processing*, vol. 21, no. 4, pp. 1756–1769, 2012.
[39] C. O. Ancuti, C. Ancuti, C. De Vleeschouwer, and P. Bekaert, "Color balance and fusion for underwater image enhancement," *IEEE Transactions on image processing*, vol. 27, no. 1, pp. 379–393, 2017.
[40] D. Akkaynak and T. Treibitz, "Sea-thru: A method for removing water from underwater images," in *Proceedings of the IEEE Conference on Computer Vision and Pattern Recognition*, 2019, pp. 1682–1691.
[41] C. O. Ancuti, C. Ancuti, C. De Vleeschouwer, and P. Bekaert, "Color balance and fusion for underwater image enhancement," *IEEE Transactions on Image Processing*, vol. 27, no. 1, pp. 379–393, 2018.
[42] D. Yang and J. Sun, "Proximal dehaze-net: A prior learning-based deep network for single image dehazing," in *Proceedings of the European Conference on Computer Vision (ECCV)*, 2018, pp. 702–717.

[43] L. K. Choi, J. You, and A. C. Bovik, "Referenceless prediction of perceptual fog density and perceptual image defogging," *IEEE Transactions on Image Processing*, vol. 24, no. 11, pp. 3888–3901, 2015.
[44] I. Lissner, J. Preiss, P. Urban, M. S. Lichtenauer, and P. Zolliker, "Image-difference prediction: From grayscale to color," *IEEE Transactions on Image Processing*, vol. 22, no. 2, pp. 435–446, 2012.